

# Distinguishing Dynamical Dark Matter at the LHC

Keith R. Dienes<sup>1,2,3\*</sup>, Shufang Su<sup>3†</sup>, Brooks Thomas<sup>4‡</sup>

<sup>1</sup> *Physics Division, National Science Foundation, Arlington, VA 22230 USA*

<sup>2</sup> *Department of Physics, University of Maryland, College Park, MD 20742 USA*

<sup>3</sup> *Department of Physics, University of Arizona, Tucson, AZ 85721 USA*

<sup>4</sup> *Department of Physics, University of Hawaii, Honolulu, HI 96822 USA*

Dynamical dark matter (DDM) is a new framework for dark-matter physics in which the dark sector comprises an ensemble of individual component fields which collectively conspire to act in ways that transcend those normally associated with dark matter. Because of its non-trivial structure, this DDM ensemble — unlike most traditional dark-matter candidates — cannot be characterized in terms of a single mass, decay width, or set of scattering cross-sections, but must instead be described by parameters which describe the collective behavior of its constituents. Likewise, the components of such an ensemble need not be stable so long as lifetimes are balanced against cosmological abundances across the ensemble as a whole. In this paper, we investigate the prospects for identifying a DDM ensemble at the LHC and for distinguishing such a dark-matter candidate from the candidates characteristic of traditional dark-matter models. In particular, we focus on DDM scenarios in which the component fields of the ensemble are produced at colliders alongside some number of Standard-Model particles via the decays of additional heavy fields. The invariant-mass distributions of these Standard-Model particles turn out to possess several unique features that cannot be replicated in most traditional dark-matter models. We demonstrate that in many situations it is possible to differentiate between a DDM ensemble and a traditional dark-matter candidate on the basis of such distributions. Moreover, many of our results also apply more generally to a variety of other extensions of the Standard Model which involve multiple stable or metastable neutral particles.

## I. INTRODUCTION

Recently, a new framework for dark-matter physics has been proposed [1, 2]. This new framework is called “dynamical dark matter” (DDM), and previous discussions of DDM have focused on its overall theoretical properties [1] as well as on the theoretical and phenomenological implications of a specific model [2, 3] that was constructed within this new framework. In this paper, we shall return to consideration of the general DDM framework as a whole, and discuss the detection prospects for a broad class of DDM models at colliders, and in particular at the Large Hadron Collider (LHC).

As discussed in Refs. [1, 2], the central hallmark of the dynamical dark-matter framework is that the dark sector consists not of one (or merely a few) stable dark-matter particles, but rather an *ensemble* of constituents which act collectively in ways that transcend the physics normally associated with more traditional dark sectors. Such a DDM ensemble is not randomly assembled, but instead has certain internal structures which guarantee its phenomenological viability. For example, stability on cosmological time scales — normally considered to be a sacrosanct property for traditional dark-matter candidates — is not a requirement for such an ensemble. Instead, lifetimes are balanced against cosmological abundances across the different constituents of this ensemble in such a way that those components with larger decay widths (and consequently shorter lifetimes) necessarily have smaller cosmological abundances, and vice versa. Indeed, as discussed in Refs. [2, 3], this balancing represents a novel way of satisfying phenomenological bounds on the dark sector without imposing stability as a whole, and ultimately represents the most general dark sector that can be imagined.

Most traditional dark-matter candidates can be characterized in terms of their masses and couplings to Standard-Model (SM) states, and indeed most phenomenological bounds in the dark-matter literature are phrased in terms of constraints on these variables [4]. By contrast, in the DDM framework the dark-matter “candidate” is the entire ensemble, and the parameters which ultimately characterize a DDM ensemble describe not only the couplings of its individual constituents to SM states, but also the internal structure of the ensemble itself. In general, such an internal structure might consist of relationships between the masses, relic abundances, and couplings of its components. As a result, the natural parameters which characterize DDM models and their phenomenology are fundamentally different

---

\* E-mail address: [dienes@physics.arizona.edu](mailto:dienes@physics.arizona.edu)

† E-mail address: [shufang@physics.arizona.edu](mailto:shufang@physics.arizona.edu)

‡ E-mail address: [thomasbd@phys.hawaii.edu](mailto:thomasbd@phys.hawaii.edu)

from those which suffice to describe traditional dark-matter candidates. Indeed, the most fundamental parameters which characterize a DDM ensemble are those which describe how quantities such as the constituent-particle masses, abundances, decay widths, and cross-sections scale with respect to one another across the ensemble as a whole. This clearly represents a new way of thinking about a dark sector, but the need for such an approach is one of the primary features of the DDM framework.

In this paper, we shall focus on the implications of these fundamental differences for the collider phenomenology of DDM ensembles, and in particular for their discovery potential at the LHC. The canonical channels in which one generally expects to obtain evidence for a DDM ensemble involve substantial missing transverse energy (hereafter denoted  $\cancel{E}_T$ ) — just as is the case for a traditional dark-matter candidate. It is therefore crucial to develop strategies for distinguishing between these two classes of models once an excess in one or more of these  $\cancel{E}_T$  channels has been identified. One such strategy, which was discussed in Ref. [3], is to search for correlations between  $\cancel{E}_T$  signatures and signals in other channels to which the DDM ensemble might simultaneously give rise — channels not normally associated with dark matter. Indeed, in DDM models, only those portions of the DDM ensemble which are stable on collider time scales contribute to missing-energy signals at colliders. By contrast, it is possible that other portions of the DDM ensemble will have much shorter lifetimes and therefore manifest themselves in different channels entirely — channels that may not involve  $\cancel{E}_T$  whatsoever. As discussed in Ref. [3], a wide variety of DDM scenarios generically give rise to observable excesses in both classes of channels simultaneously. However, in a variety of other DDM contexts, such correlations among channels may not be possible due to the particulars of the model and the lifetimes of the constituent fields in the ensemble. In such contexts — and especially when those constituent fields manifest themselves only through  $\cancel{E}_T$  signatures — alternative strategies for identifying DDM ensembles are necessary.

Such alternative strategies will be the primary focus of this paper. In particular, one of our central aims is to demonstrate that in many cases it is possible to distinguish DDM ensembles from more traditional dark-matter candidates based solely on results from channels in which the dark-matter particles manifest themselves as  $\cancel{E}_T$  alone. For example, the invariant-mass distributions of SM states produced in association with the constituent fields in a DDM ensemble by the decays of heavy particles can exhibit qualitative features which transcend those usually associated with traditional dark-matter candidates. As we shall see, such invariant-mass distributions can therefore provide a powerful experimental discriminant between DDM ensembles and these traditional candidates. Furthermore, because this technique relies solely on signatures in detection channels in which the component fields of the DDM ensemble appear as  $\cancel{E}_T$ , these signatures are insensitive to the precise lifetimes of any component fields which leave an imprint on the invariant-mass distribution in question. Hence, they are likewise insensitive to the characteristic instability of the DDM ensemble as a whole, and this remains true provided that these fields are all sufficiently long-lived so as not to decay within the detector volume. These aspects of our discussion therefore have a broad applicability even beyond the context of the DDM framework, and apply quite generally to any multi-component dark-matter scenario involving an additional heavy “parent” particle which decays to final states involving the dark-sector fields, or to any scenario involving multiple metastable neutral fields and such a parent particle.

In order to explicitly illustrate these themes, in this paper we shall consider the case in which each parent particle decays directly to a single constituent field within the DDM ensemble along with a pair of strongly-interacting SM particles (*i.e.*, quarks or gluons). Even in this simplest non-trivial case, we shall demonstrate that there exist a range of characteristic features which are imprinted on the invariant-mass distribution of the two resulting jets and which can permit one to distinguish a DDM ensemble from any traditional dark-matter candidate. Moreover, we shall show that there exist production mechanisms for the parent particles (such as pair-production via strong interactions) with event rates sufficient to enable such a differentiation at the  $5\sigma$  significance level within the first  $30 \text{ fb}^{-1}$  of integrated luminosity at the  $\sqrt{s} = 14 \text{ TeV}$  LHC.

This paper is organized as follows. In Sect. II, we outline the general aspects of the collider phenomenology of DDM ensembles and discuss the strategies for indirectly observing those ensembles in different classes of DDM models from the perspective of effective-operator analysis. In doing so, we devote particular attention to models in which the component particles in the DDM ensemble are produced via the decays of a heavy parent particle. In Sect. III, we calculate the invariant-mass distributions associated with pairs of SM states produced in conjunction with each dark-matter particle via this mechanism and compare them to the invariant-mass distributions obtained in theories involving only a single particle stable on collider time scales. In Sect. IV, we assess the statistical significance with which such non-traditional invariant-mass distributions can be distinguished from those in more traditional dark-matter models. In Sect V, we provide an example of one production mechanism which naturally provides event rates of the order required for such a differentiation within the first  $30 \text{ fb}^{-1}$  of integrated luminosity at the  $\sqrt{s} = 14 \text{ TeV}$  LHC — namely, the pair-production of strongly-interacting parent particles with masses near the TeV scale. Finally, in Sect VI, we provide an assessment of how various subtleties associated with certain production mechanisms for the parent particle (such as the combinatorial background associated with incorrect pairings of final-state jets for processes which yield more than one such parent particle per event) are expected to impact our results. We also comment on the broader applicability of our results to scenarios outside the DDM framework.

## II. DYNAMICAL DARK MATTER AT THE LHC: GENERAL CONSIDERATIONS

One of the hallmarks of the DDM framework is that the dark sector consists of an ensemble of particles  $\chi_n$ , where  $n = \{0, \dots, N\}$ , with  $N$  presumed to be relatively large, *i.e.*,  $N \gg 1$ . For convenience, we shall label these particles in order of increasing mass, *i.e.*,  $m_{n+1} \geq m_n$ . Moreover, as discussed in Refs. [1–3], these particles  $\chi_n$  exhibit a broad spectrum of decay widths  $\Gamma_n$  which scale inversely with their corresponding cosmological abundances  $\Omega_n$ . As a result of these different decay widths, different  $\chi_n$  may manifest themselves in qualitatively different ways at colliders — even in situations in which the  $\chi_n$  all have similar quantum numbers and are therefore produced via similar processes. Those  $\chi_n$  with lifetimes  $\tau_n \gtrsim 10^{-10}$  s are stable on collider time scales and appear in a collider detector as  $\cancel{E}_T$ . By contrast, any of the  $\chi_n$  with lifetimes  $\tau_n \lesssim 10^{-10}$  s decay within the detector volume. Provided these rapidly-decaying  $\chi_n$  decay predominately to final states involving SM particles, evidence for a DDM ensemble could potentially be obtained via the observation of signals in complementary channels which individually provide evidence for  $\chi_n$  within either of these  $\tau_n$  regimes. Such signatures are discussed in Ref. [3]. However, for models in which  $\tau_n \gtrsim 10^{-10}$  s for all  $\chi_n$  — or for models in which the  $\chi_n$  that decay within the detector volume are not collectively produced at rates sufficient to yield observable effects at colliders — such multi-channel correlation techniques are not useful. In such cases, alternative strategies must be found for distinguishing DDM models from more traditional dark-matter models.

In this paper, we will examine one such strategy, which is applicable to a broad class of DDM models possessing two key characteristics. First, in addition to the constituent fields  $\chi_n$  of the DDM ensemble, the field content of the model must include one or more heavy particles  $\psi$  which can be produced at a substantial rate at a hadron collider. For example, if the  $\psi$  transform non-trivially under the SM  $SU(3)_c$  gauge group, they can be produced copiously via their interactions with the quark and gluon fields. Second, these additional, heavy particles must decay with a sizeable branching fraction into final states including at least two SM fields, along with one or more of the  $\chi_n$ . Decay topologies of this sort arise generically, for example, in a specific class of DDM scenarios in which both the parent particle  $\psi$  and the constituents of the DDM ensemble are charged under an approximate symmetry. However, in such cases it is an important property of the general DDM framework that such a symmetry is neither required nor need be preserved exactly. Therefore, the ensemble constituents need not ultimately be stable.

We shall demonstrate that it is possible to differentiate between traditional, single-particle models of dark matter and multi-component scenarios, such as those which arise in the DDM framework, by examining the invariant-mass distributions of the SM fields produced by  $\psi$  decays. Of course, in cases in which only a small number of the  $\chi_n$  are kinematically accessible in  $\psi$  decays, these invariant-mass distributions are distinguished by the presence of multiple kinematic edges. Note that similar features arise in other contexts as well, most notably that in which a parent particle can decay into final states involving different *multiplicities* of the same stable dark-matter particle [5, 6]. By contrast, in cases in which the number of kinematically-accessible  $\chi_n$  is large and the decay phenomenology of the  $\psi$  particles depends more sensitively on the full structure of the DDM ensemble, qualitatively different features emerge. In particular, while individual kinematic edges are no longer manifest, the invariant-mass distributions can exhibit distinctive shapes not realized in single-particle dark-matter scenarios. These distributions can therefore provide a powerful experimental discriminant between DDM ensembles and more traditional dark-matter candidates.

We note that the technique described above has a broad range of applicability because it is not predicated on the observation of signals of both collider-stable and promptly-decaying  $\chi_n$ , but rather of collider-stable fields alone. Moreover, for the same reason, this technique can also be applied more broadly to a wide variety of multi-component dark-matter models, or to other scenarios which involve multiple particles which are stable on collider time scales. Such situations can arise in certain limits of traditional dark-matter scenarios in which the dark-matter candidate is stabilized by a parity symmetry such as  $R$ -parity in supersymmetric models or KK parity [7] in higher-dimensional theories in which the SM propagates in the bulk [8–10]. For example, while only the lightest parity-odd particle is absolutely stable in such scenarios, situations can arise in which the decay rates of heavier parity-odd particles with similar quantum numbers are suppressed (either by kinematics or by some additional consideration) to such an extent that they are also stable on collider time scales. In such cases, the invariant-mass distributions associated with the decays of even heavier fields in the theory include contributions from final states involving *all* such stable or metastable particles. These distributions can therefore yield valuable information about the overall coupling structure and mass spectrum of the theory.

In order to analyze the collider phenomenology of DDM ensembles, it is first necessary to characterize the properties of such dark-matter candidates in a straightforward and physically meaningful manner. Indeed, a DDM ensemble is not a single particle or a small group of particles, but rather a vast collection of individual states whose collective properties dictate the dark-matter phenomenology of the model. Taken together, therefore, an ensemble of such states constitutes a dark-matter candidate which cannot be characterized in terms of a single well-defined mass, decay width, or set of cross-sections for processes involving SM fields. Instead, a DDM ensemble is more aptly characterized by parameters which describe its aggregate internal structure. Such parameters may include, for example, scaling exponents in certain relations between masses and cross-sections, or between cosmological abundances and decay

widths, that hold across the DDM ensemble as a whole. More specifically, one natural set of such parameters might include the density of states expressed as a function of the masses  $m_n$  of the  $\chi_n$ , and a set of exponents which describe the scaling behavior of the couplings of the  $\chi_n$  to other fields present in the theory.

In any arbitrary DDM model, such couplings can be described by a set of operators  $\mathcal{O}_{n_1, n_2, \dots}^{(\alpha)}$ , where the indices  $n_i$  indicate the dark-sector fields  $\chi_{n_i}$  involved and where the index  $\alpha$  labels the operator in question. We shall let  $d_\alpha$  denote the mass dimension of the operator  $\mathcal{O}_{n_1, n_2, \dots}^{(\alpha)}$ . We shall assume for the sake of simplicity in what follows that the only  $\mathcal{O}_{n_1, n_2, \dots}^{(\alpha)}$  which play a meaningful role in the collider phenomenology of the DDM ensemble are members of the subset  $\mathcal{O}_n^{(\alpha)}$  of operators which involve only a single  $\chi_n$ . We therefore have an effective interaction Lagrangian of the form

$$\mathcal{L}_{\text{eff}} = \sum_{\alpha} \sum_{n=0}^N \frac{c_{n\alpha}}{\Lambda^{d_\alpha-4}} \mathcal{O}_n^{(\alpha)} + \dots, \quad (2.1)$$

where  $\Lambda$  is the cutoff scale of the effective theory, and where  $c_{n\alpha}$  is the dimensionless operator coefficient associated with  $\mathcal{O}_n^{(\alpha)}$ . In addition, we shall also assume that all the constituent particles in the ensemble have the same quantum numbers, and thus that the set of  $\mathcal{O}_n^{(\alpha)}$  consistent with the symmetries of the theory shares a common operator structure for all  $n$ . In other words, for any given  $\alpha$ , the only  $n$ -dependence appears in the mass  $m_n$  of the field  $\chi_n$  and the coefficient  $c_{n\alpha}$ . Furthermore, we assume that the distribution of  $c_{n\alpha}$  across the ensemble depends solely on  $m_n$ , and that both this distribution and the mass spectrum of the ensemble exhibit general scaling relations of the form

$$\begin{aligned} m_n &= m_0 + n^\delta \Delta m \\ c_{n\alpha} &= c_{0\alpha} \left( \frac{m_n}{m_0} \right)^{\gamma_\alpha}, \end{aligned} \quad (2.2)$$

where the (positive) mass-splitting parameter  $\Delta m$  and the scaling exponents  $\delta$  and  $\gamma_\alpha$  are free parameters. Note that  $\delta > 0$  by construction. All of these assumptions can, of course, be relaxed; however, the qualitative results obtained below still continue to hold in more general cases as well. Note that the  $\mathcal{O}_n^{(\alpha)}$  are ultimately responsible both for the production of the  $\chi_n$  at colliders, and for their decay phenomenology — both in terms of their lifetimes  $\tau_n$  and in terms of their decay products. Of course the  $\mathcal{O}_n^{(\alpha)}$  which play a dominant role in the production of the  $\chi_n$  need not be the same as those which play a dominant role in determining their decay properties.

In this paper we shall focus primarily on the  $\chi_n$  which are stable on collider time scales, as discussed above; hence our primary concern in what follows will be with production rather than decay. In fact, given the scaling relations and parameterizations in Eqs. (2.1) and (2.2), we can now characterize precisely which components of a given DDM ensemble contribute to  $\cancel{E}_T$  signals once produced. Assuming that a given  $\chi_n$  decays primarily to final states comprising SM fields the sum of whose masses is much smaller than  $m_n$ , we find that  $\Gamma_n$  scales roughly like

$$\Gamma_n \sim \sum_{\alpha} c_{n\alpha}^2 \frac{m_n^{2d_\alpha-7}}{\Lambda^{2d_\alpha-8}}. \quad (2.3)$$

As discussed above, the distribution of  $\Gamma_n$  across the DDM ensemble has a significant impact not only on the cosmological aspects of that ensemble, but on its collider phenomenology as well. When the lifetime  $\tau_n = 1/\Gamma_n$  of the particle is short on collider time scales ( $\tau_n \lesssim 10^{-12}$  s), the particle decays promptly within the detector. When the lifetime is long ( $\tau_n \gtrsim 10^{-10}$  s), the particle decays outside the detector and appears as  $\cancel{E}_T$ . In the intermediate region ( $10^{-12}$  s  $\lesssim \tau_n \lesssim 10^{-10}$  s), the particle may give rise to a displaced vertex. Thus  $\chi_n$  within different ranges of  $m_n$  in the ensemble may manifest themselves either as  $\cancel{E}_T$  or via their decay products, depending on the value of  $\Gamma_n$ . For example, in the case in which a single operator  $\mathcal{O}_n^{(\alpha)}$  governs the decay width of all relevant  $\chi_n$ , Eqs. (2.2) and (2.3) together imply that the requirement for appearing as  $\cancel{E}_T$  is

$$\Gamma_0 \left( 1 + n^\delta \frac{\Delta m}{m_0} \right)^{2d_\alpha-7+2\gamma_\alpha} \lesssim 6.58 \times 10^{-15} \text{ GeV}, \quad (2.4)$$

where  $\gamma_\alpha$  here denotes the particular scaling exponent associated with the operator which effectively controls the decay width of  $\chi_n$ , and  $\Gamma_0$  is the decay width of the lightest state in the ensemble.

### III. IMPRINTS OF DDM ENSEMBLES IN KINEMATIC DISTRIBUTIONS

By and large, when a dark-sector field is produced at the LHC via the decay of a heavy parent particle  $\psi$ , multiple SM fields can also be produced via the same decay. One useful variable that can assist in distinguishing models

involving a single dark-matter candidate from those involving more complicated dark sectors in scenarios of this sort is the invariant mass of the additional SM particles produced by decays of the parent particle. The identification of features in invariant-mass distributions has been shown to be effective in differentiating between the different symmetries which might stabilize a dark-matter particle in traditional dark-matter models [5]. In this paper, we show that it is also effective in distinguishing between traditional and DDM dark sectors.

For purposes of illustration, we focus on the case in which each  $\psi$  decay yields two SM particles and a single  $\chi_n$ . Indeed, this is the simplest case in which a non-trivial invariant-mass distribution is obtained for the SM particles from the decay of a single  $\psi$ . Furthermore, since strongly-interacting particles can be produced copiously at colliders, we shall focus on the case in which  $\psi$  carries  $SU(3)_c$  charge and decays to a pair of SM quarks or gluons which form hadronic jets, and the relevant kinematic variable is the invariant mass  $m_{jj}$  of the two jets thus produced. We assume that each  $\psi$  decays primarily via three-body processes of the form  $\psi \rightarrow jj\chi_n$ . We discuss the alternative possibility in which  $\psi$  decays to the same final state through cascade decays involving a on-shell intermediary in Sect. VI. Finally, we assume here for simplicity that the pair of final-state jets produced via the decay of each particular  $\psi$  can be correctly identified in each event. Such an identification is trivial in situations such as those in which  $\psi$  is produced singly or in which there exist other decay channels for  $\psi$  with branching fractions similar to  $\sum_n \text{BR}(\psi \rightarrow jj\chi_n)$  whose decay products are readily distinguishable from jets. However, if no such alternative decay channels exist — *i.e.*, if decays of the form  $\psi \rightarrow jj\chi_n$  dominate the width of  $\psi$  — the analysis becomes significantly more complex because of the non-trivial combinatorial issues which arise due to the possibility of incorrect pairings among the final-state jets. However, a number of techniques have been developed which can assist in identifying the correct jet pairings in such situations. We shall discuss these techniques, and the effect of combinatorial issues in general, in more detail in Sect. VI.

We begin our analysis of the invariant-mass distributions which arise in the context of the DDM framework by briefly reviewing the characteristics of the corresponding distributions which arise in traditional dark-matter models. This will be important for purposes of comparison when we consider the contrasting case of a full DDM ensemble. Towards this end, let us consider a traditional dark-matter model in which a parent particle  $\psi$  likewise decays predominately into a three-body final state comprising a dark-matter particle  $\chi$  and a pair of strongly-interacting SM fields (either quarks or gluons). The latter appear in the detector as hadronic jets, here labeled  $j_1$  and  $j_2$ . Irrespective of the Lorentz or  $SU(3)_c$  representations of these fields, the differential partial width  $d\Gamma_\psi \equiv d\Gamma(\psi \rightarrow j_1 j_2 \chi)$  associated with this decay channel is given by the general three-body decay-width formula

$$d\Gamma_\psi = \frac{1}{32(2\pi)^3 m_\psi^3} |\overline{\mathcal{M}}|^2 dm_{jj}^2 dm_{j_2\chi}^2, \quad (3.1)$$

where  $|\overline{\mathcal{M}}|^2$  is the matrix element for the parton-level process (averaged over the spin and color states of  $\psi$ ),  $m_{jj}$  is the invariant mass of  $j_1$  and  $j_2$ , and  $m_{j_2\chi}$  is the invariant mass of  $j_2$  and  $\chi$ . The normalized invariant-mass distribution associated with these decays is therefore given by

$$\frac{1}{\Gamma_\psi} \frac{d\Gamma_\psi}{dm_{jj}} = \frac{m_{jj}}{16(2\pi)^3 m_\psi^3 \Gamma_\psi} \int_{m_-^2}^{m_+^2} |\overline{\mathcal{M}}|^2 dm_{j_2\chi}^2, \quad (3.2)$$

where the limits of integration are

$$m_\pm^2 \equiv \frac{1}{2} \left[ m_\psi^2 + m_\chi^2 - m_{jj}^2 \pm \sqrt{m_\psi^4 - 2m_\psi^2(m_\chi^2 + m_{jj}^2) + (m_{jj}^2 - m_\chi^2)^2} \right] \quad (3.3)$$

in the limit that parton masses can be neglected. Note that Eq. (3.2) vanishes for  $m_{jj} = 0$  and for  $m_{jj} = m_\psi - m_\chi$ .

The explicit form of the  $m_{jj}$  distribution which arises in any particular model depends on the coupling structure between  $\psi$ ,  $\chi$ , and the SM quark or gluon fields. As a concrete example, let us consider the case in which  $\chi$  and  $\psi$  are both fermions, and  $\psi$  transforms in the octet representation of  $SU(3)_c$ , while  $\chi$  is neutral under all SM symmetries. In this case,  $\psi$  can decay via the effective four-fermion interaction term

$$\mathcal{L}_{\text{eff}} = \frac{c}{\Lambda^2} (\bar{q}_i t_{ij}^a \psi^a) (\bar{\chi} q_j) + \text{h.c.} \quad (3.4)$$

where  $q$  denotes a SM quark,  $t_{ij}^a$  is the generator of  $SU(3)$  in the fundamental representation, the indices  $i$  and  $j$  label the states in the fundamental representation, and  $a$  labels the states in the adjoint representation. The spin- and color-averaged squared matrix element for an interaction of this form is then given by

$$|\overline{\mathcal{M}}|^2 = \frac{c^2}{\Lambda^4} (m_\psi^2 - m_{j_2\chi}^2)(m_{j_2\chi}^2 - m_\chi^2). \quad (3.5)$$

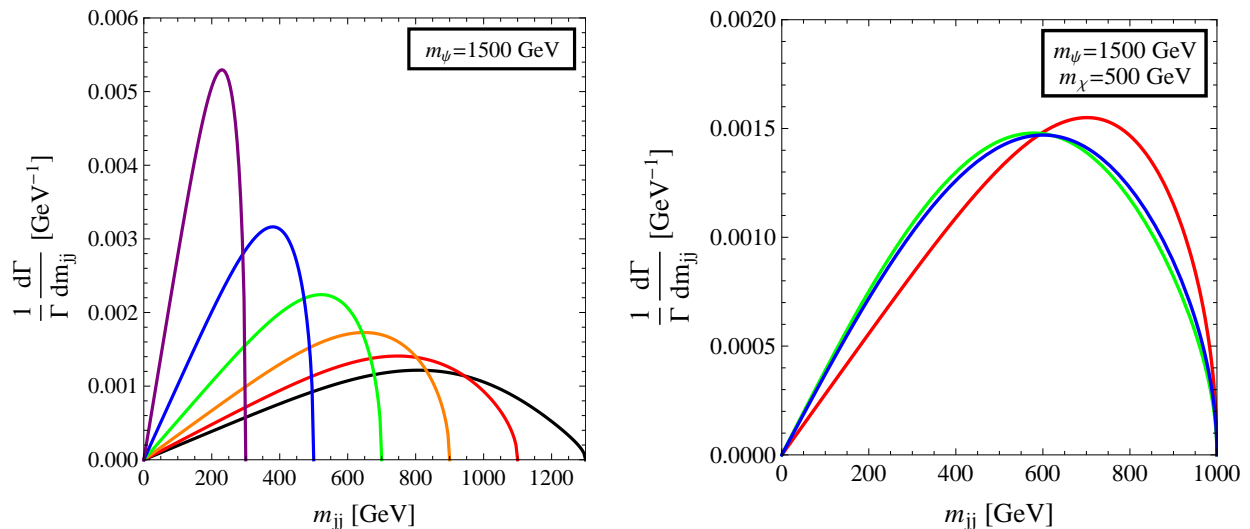


FIG. 1: Characteristic invariant-mass distributions in the traditional dark-matter models discussed in the text. The left panel shows the normalized dijet invariant-mass distributions associated with the decays of a heavy octet fermion  $\psi$  with a mass  $m_\psi = 1500$  GeV to a quark-antiquark pair and a single dark-matter candidate with a mass  $m_\chi$ . The black, red, orange, green, blue, and purple curves correspond respectively to  $m_\chi = \{200, 400, 600, 800, 1000, 1200\}$  GeV. The right panel shows the distributions for fixed  $m_\psi = 1500$  GeV and  $m_\chi = 500$  GeV, but for  $\psi$  and  $\chi$  with different spins and transformation properties under  $SU(3)_c$  and therefore different coupling structures with the SM fields. The red curve corresponds to the parton-level process  $\psi \rightarrow q\bar{q}\chi$  in which  $\psi$  and  $\chi$  are both fermions, the green curve corresponds to the process  $\psi \rightarrow qq\chi$  in which  $\psi$  and  $\chi$  are both scalars, and the blue curve corresponds to the process  $\psi \rightarrow gq\chi$  in which  $\psi$  is a fermion and  $\chi$  is a scalar. We observe that coupling structure does not induce a dramatic change in the dijet invariant-mass distribution.

In the left panel of Fig. 1, we display the  $m_{jj}$  distributions obtained in this case for  $m_\psi = 1500$  GeV and several different choices of  $m_\chi$ . Note that each distribution shown features a characteristic mass edge at the kinematic endpoint  $m_{jj} = m_\psi - m_\chi$ , which differs for each  $m_\chi$ . However, in most other aspects, the distributions are qualitatively quite similar, and in particular have the same overall shape.

Of course, different coupling structures from the one specified in Eq. (3.4) correspond to different functional forms for  $|\overline{\mathcal{M}}|^2$ , and one might wonder what effect such differences in coupling structure have on the  $m_{jj}$  distribution as a whole. In the right panel of Fig. 1, we compare the  $m_{jj}$  distributions associated with several allowed combinations of Lorentz and  $SU(3)_c$  representations for both parent and daughter particles, which result in different coupling structures. The distributions shown correspond to the parton-level process  $\psi \rightarrow q\bar{q}\chi$  for which  $\psi$  and  $\chi$  are both fermions (red), the process  $\psi \rightarrow qq\chi$  for which  $\psi$  and  $\chi$  are both scalars (green), and the process  $\psi \rightarrow gq\chi$  for which  $\psi$  is a fermion and  $\chi$  is a scalar (blue). These decay processes arise in the cases in which  $\psi$  transforms as an **8**, as a **6**, and as a **15** under  $SU(3)_c$ , respectively. In each case, we have set  $m_\psi = 1500$  GeV and  $m_\chi = 500$  GeV. While these distributions vary slightly from one another, we once again see that they all have essentially the same shape, which includes a characteristic mass edge at  $m_{jj} = m_\psi - m_\chi$ . Indeed, we observe that the  $m_{jj}$  distributions do not differ dramatically among single-particle dark-matter models as a result of differences in coupling structure.

We now consider how the decay phenomenology of  $\psi$  in the context of the DDM framework differs from that associated with the traditional dark-matter scenarios discussed above. As we shall see, while each individual constituent  $\chi_n$  in the DDM ensemble contributes to the width of  $\psi$  and to the overall  $m_{jj}$  distribution in a manner analogous to a traditional dark-matter candidate, the collective behavior of these  $\chi_n$  gives rise to distinctly new phenomena. For concreteness, we once again focus on the particular case in which  $\psi$  is a color-octet fermion and the  $\chi_n$  are fermions which transform as singlets under the SM gauge group; however, as the right panel of Fig. 1 attests, the shape of the  $m_{jj}$  distributions does not depend sensitively on the spins of the particles involved or the structure of the interaction vertex, and the results obtained for different cases will therefore be analogous. We focus on the case in which  $\psi \rightarrow jj\chi_n$  decays arise predominately due to a four-fermion interaction analogous to Eq. (3.4):

$$\mathcal{L}_{\text{eff}} = \sum_n \left[ \frac{c_n}{\Lambda^2} (\bar{q}_i t_{ij}^a \psi^a) (\bar{\chi}_n q_j) + \text{h.c.} \right]. \quad (3.6)$$

For convenience, we shall henceforth use the symbol  $\gamma$  to denote the particular scaling exponent  $\gamma_\alpha$  associated with

this operator, so that the operator coefficients  $c_n$  scale according to the relation

$$c_n = c_0 \left( \frac{m_n}{m_0} \right)^\gamma, \quad (3.7)$$

in the manner described in Eq. (2.2). We will also assume for simplicity that there are no additional decay channels for  $\psi$ , and that the sum of the branching fractions for all decays of the form  $\psi \rightarrow jj\chi_n$  is effectively unity. Moreover, we will assume that the operators which contribute to the decay widths of all  $\chi_n$  with masses  $m_n < m_\psi$  are sufficiently suppressed so that all such particles amply satisfy the condition in Eq. (2.4) and therefore manifest themselves as  $\cancel{E}_T$ .

For the coupling structure specified in Eq. (3.6), the differential decay width  $d\Gamma_{\psi n} \equiv \Gamma(\psi \rightarrow \bar{q}q\chi_n)$  for  $\psi$  decay into any particular  $\chi_n$  is likewise given by Eq. (3.1), and  $|\overline{\mathcal{M}}|^2$  is given by

$$|\overline{\mathcal{M}}|^2 = \frac{c_n^2}{\Lambda^4} (m_\psi^2 - m_{j_2 n}^2)(m_{j_2 n}^2 - m_n^2), \quad (3.8)$$

where  $m_{j_2 n}$  denotes the invariant mass of  $\chi_n$  and  $j_2$ . Integrating over  $dm_{j_2 n}^2$  yields the differential *partial* decay width of  $\psi$  with respect to  $m_{jj}$  for the particular decay  $\psi \rightarrow jj\chi_n$ :

$$\frac{d\Gamma_{\psi n}}{dm_{jj}} = \frac{c_n^2 m_{jj} \sqrt{m_\psi^4 - 2m_\psi^2(m_{jj}^2 + m_n^2) + (m_{jj}^2 - m_n^2)}}{96(2\pi)^3 m_\psi^3 \Lambda^4} \left[ m_\psi^4 + m_\psi^2(m_{jj}^2 - 2m_n^2) - 2m_{jj}^4 + m_{jj}^2 m_n^2 + m_{jj}^4 \right]. \quad (3.9)$$

The partial width for  $\psi \rightarrow jj\chi_n$  is therefore

$$\Gamma_{\psi n} = \frac{c_n^2}{384(2\pi)^3 \Lambda^4 m_\psi^3} \left[ m_\psi^8 - 8m_\psi^2 m_n^2 (m_\psi^4 - m_n^4) + 12m_\psi^4 m_n^4 \ln \left( \frac{m_n^2}{m_\psi^2} \right) \right]. \quad (3.10)$$

Since the products of each such decay mode appear in a collider detector as a pair of jets plus  $\cancel{E}_T$ , the *total* differential dijet invariant-mass distribution observed is a sum of the  $m_{jj}$  distributions for each channel, weighted by the corresponding decay branching fraction:

$$\frac{1}{\Gamma_\psi} \frac{d\Gamma_\psi}{dm_{jj}} = \sum_{n=0}^{n_{\max}} \left( \frac{1}{\Gamma_{\psi n}} \frac{d\Gamma_{\psi n}}{dm_{jj}} \times \text{BR}_{\psi n} \right), \quad (3.11)$$

where  $\Gamma_\psi \equiv \sum_n \Gamma_{\psi n}$  is the total contribution to the decay width of  $\psi$  from processes of the form  $\psi \rightarrow jj\chi_n$ , where  $\text{BR}_{\psi n} \equiv \Gamma_{\psi n}/\Gamma_\psi$  denotes the branching fraction for the particular decay  $\psi \rightarrow jj\chi_n$ , where  $n_{\max}$  is the value of  $n$  corresponding to the heaviest  $\chi_n$  kinematically accessible in  $\psi$  decay. Note that this result also applies in the case in which other decay channels exist for  $\psi$  with distinguishable final states. The invariant-mass distribution in Eq. (3.11) therefore depends not only on the parameters  $\Delta m$  and  $\delta$  (which control the mass spectrum of the  $\chi_n$  and therefore the available phase space for each individual decay channel), but also the parameter  $\gamma$  (which affects the branching fractions associated with these channels).

In order to explicitly illustrate the dependence of the branching fractions  $\text{BR}_{\psi n}$  on  $\delta$ ,  $\gamma$ , and  $\Delta m$ , in Fig. 2 we display  $\text{BR}_{\psi n}$  as a function of  $n$ . In each of the three panels shown, we have taken  $m_\psi = 1500$  GeV and  $m_0 = 200$  GeV. The curves in the left panel correspond to different choices of  $\Delta m$  for fixed  $\gamma = 0$  and  $\delta = 1$ ; this represents a case in which the mass splitting between the  $\chi_n$  is uniform and each of these particles couples to  $\psi$  with equal strength. In this case, the dependence of the branching fraction on  $n$  is solely due to the available phase space for  $\psi \rightarrow jj\chi_n$  decays, which decreases monotonically with  $n$  up to the kinematic limit — *i.e.*, so long as  $m_n \leq m_\psi$  — above which  $\text{BR}_{\psi n} = 0$ . For large values of  $\Delta m$ , we see that only a few states are kinematically accessible, and the branching fractions to the heavier states are significantly suppressed. By contrast, for small  $\Delta m$ , a large number of states are kinematically accessible, and  $\text{BR}_{\psi n}$  decreases quite gradually with increasing  $n$ . A similar effect is manifest in the center panel of Fig. 2, in which the curves correspond to different values of  $\delta$  for fixed  $\gamma = 0$  and  $\Delta m = 50$  GeV. However, since increasing  $\delta$  has the effect of increasing the mass gap between the  $\chi_n$ , we see that  $\text{BR}_{\psi n}$  drops more rapidly with  $n$  when  $\delta$  is large.

Finally, in the right panel of Fig. 2, we display curves which correspond to different values of  $\gamma$  for fixed  $\delta = 1$  and  $\Delta m = 50$  GeV. For  $\gamma \leq 0$ , we observe that  $\text{BR}_{\psi n}$  decreases monotonically with  $n$  as in the left and center panels, since such values of  $\gamma$  simply imply an additional coupling suppression of  $\text{BR}_{\psi n}$  for the heavy states in addition to the phase-space suppression discussed above. By contrast, the couplings of the heavy states are *enhanced* for  $\gamma > 0$ , and the effect of this coupling enhancement and the phase-space suppression compete. As a result, in this case, the dominant decay mode for  $\psi$  may not be to the lightest state in the ensemble, but rather to a more massive state.

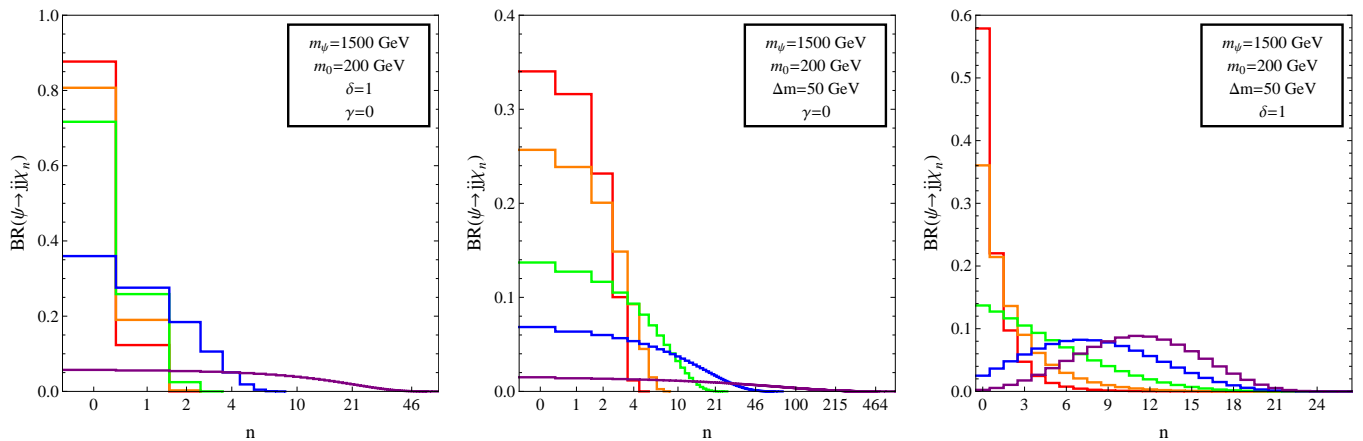


FIG. 2: The branching fraction  $\text{BR}(\psi \rightarrow jj\chi_n)$ , plotted as a function of the DDM-ensemble index  $n$ . In all cases we have taken  $m_\psi = 1500$  GeV and  $m_0 = 200$  GeV. In the left panel, we have set  $\delta = 1$  and  $\gamma = 0$ , and the red, orange, green, blue, and purple curves correspond respectively to  $\Delta m = \{600, 500, 400, 150, 20\}$  GeV. In the center panel, we have set  $\Delta m = 50$  GeV and  $\gamma = 0$ , and the same colors respectively correspond to  $\delta = \{2, 1.5, 1, 0.75, 0.5\}$ . In the right panel, we have set  $\Delta m = 50$  GeV and  $\delta = 1$ , and the same colors respectively correspond to  $\gamma = \{-2, -1, 0, 1, 2\}$ . Note that the left and center panels show the DDM index  $n$  on a log scale, while the right panel shows  $n$  on a linear scale.

Having examined how the branching fractions  $\text{BR}_{\psi n}$  depend on the parameters  $\Delta m$ ,  $\delta$ , and  $\gamma$  which characterize our DDM ensemble, we now turn to examine how the  $m_{jj}$  distributions themselves depend on these parameters. In Fig. 3, we illustrate how these distributions depend on  $\gamma$  and  $\Delta m$  for fixed  $m_\psi = 1500$  GeV,  $m_0 = 200$  GeV, and  $\delta = 1$ . The results shown in the left, center, and right panels correspond to  $\gamma = \{-1, 0, 1\}$ , respectively. The red, orange, green, and blue curves in each panel respectively correspond to the mass splittings  $\Delta m = \{600, 400, 150, 20\}$  GeV, while the black curve corresponds to the limiting case in which  $\Delta m \rightarrow \infty$ , or equivalently to the case of a single dark-matter candidate with mass  $m_\chi = m_0$ .

It is evident from Fig. 3 that in cases in which  $\gamma < 0$ , the heavier fields in the DDM ensemble couple more weakly to  $\psi$  than the lighter states, to the result that  $\chi_0$  dominates in  $\Gamma_\psi$ . However, as  $\gamma$  increases, the  $\text{BR}_{\psi n}$  for  $n > 0$  also increase, to the extent that for large  $\gamma$ , decays to the heavier states in the ensemble actually dominate the width of  $\psi$ . In this latter regime, multiple kinematic edges are evident when  $\Delta m$  is sizable. While such edges cannot be resolved when  $\Delta m$  is small, the peak of the distribution nevertheless shifts to smaller values of  $m_{jj}$ . This behavior is due to the increased branching fractions of  $\psi$  to the plethora of heavier  $\chi_n$  in the DDM ensemble which are kinematically accessible in  $\psi$  decays.

In Fig. 4, we illustrate the dependence of the  $m_{jj}$  distributions on  $\delta$  and  $\Delta m$  for fixed  $m_\psi = 1500$  GeV,  $m_0 = 200$  GeV, and  $\gamma = 1$ . The left, center, and right panels respectively correspond to the cases in  $\delta = \{0.5, 1, 3\}$ . We see from the right panel that for large  $\delta$ , and especially when  $\Delta m$  is large, the  $m_{jj}$  distribution is sensitive primarily to only the lightest few  $\chi_n$  in the DDM ensemble. As a result, the distributions shown are characterized by the presence of several identifiable mass edges, each corresponding to one of these light  $\chi_n$ . By contrast, we see in the left panel that for small  $\delta$ , a qualitatively different situation emerges: in this regime, the individual mass edges become difficult to distinguish, especially for small  $\Delta m$ , and the peaks of the invariant-mass distributions shift to lower values of  $m_{jj}$ .

Finally, in Fig. 5, we illustrate the dependence of the  $m_{jj}$  distributions on  $\delta$  and  $\gamma$  for fixed  $m_\psi = 1500$  GeV,  $m_0 = 200$  GeV, and  $\Delta m = 200$  GeV. The left, center, and right panels correspond respectively to the cases in which  $\delta = \{0.5, 1, 2\}$ . As in Fig. 4, for large  $\delta$  we see that the  $m_{jj}$  distribution is sensitive primarily to the lightest states in the ensemble and features an identifiable mass edge corresponding to each such state, while for small  $\delta$  the mass edges become increasingly indistinct. However, we also see from the left panel that the overall shape of the distribution and the location of its peak still depend on  $\gamma$ , even in situations in which no individual mass edge can be identified. Thus, even in this limit, we find that the shape of the  $m_{jj}$  distribution conveys non-trivial information about the structure of the DDM ensemble.

To summarize, we see that DDM models give rise to two characteristic classes of  $m_{jj}$  distributions in different regimes of model parameter space. Each of these represents a dramatic departure from the  $m_{jj}$  distributions typically realized in traditional dark-matter models. In the regime in which only a few states contribute significantly to the decay width of the parent particle  $\psi$ , the  $m_{jj}$  distribution is characterized by the presence of multiple identifiable mass edges. This occurs either when the mass splittings between the heavier states in the ensemble are large, due to



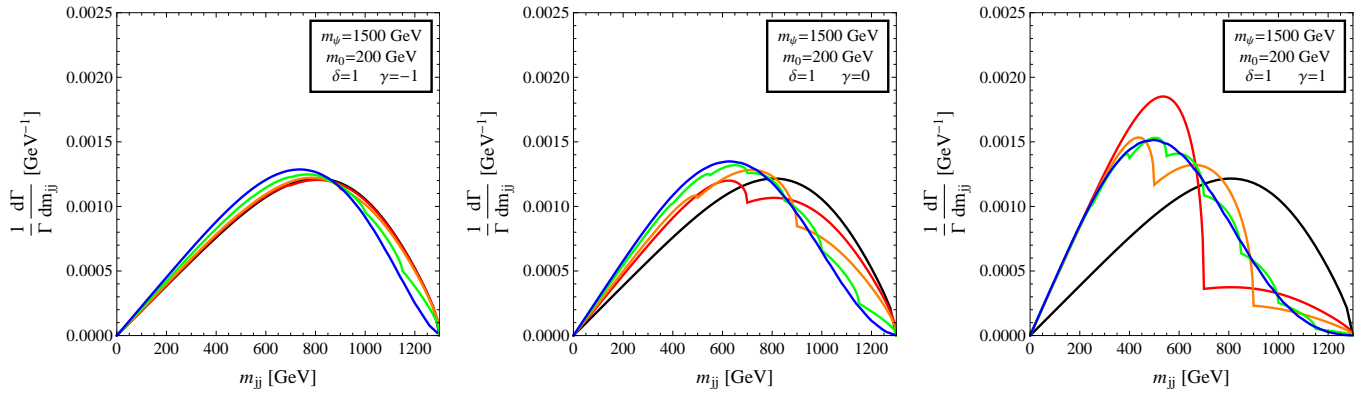


FIG. 3: DDM invariant-mass distributions, shown for increasing  $\gamma$  with fixed  $m_\psi = 1500$  GeV,  $m_0 = 200$  GeV, and  $\delta = 1$ . The results shown in the left, center, and right panels correspond to  $\gamma = \{-1, 0, 1\}$ , respectively. In each panel, the red, orange, green, and blue curves correspond to mass splittings  $\Delta m = \{600, 400, 150, 20\}$  GeV, respectively, while the black curve shows the result for a traditional dark-matter candidate with  $m_\chi = m_0$ .

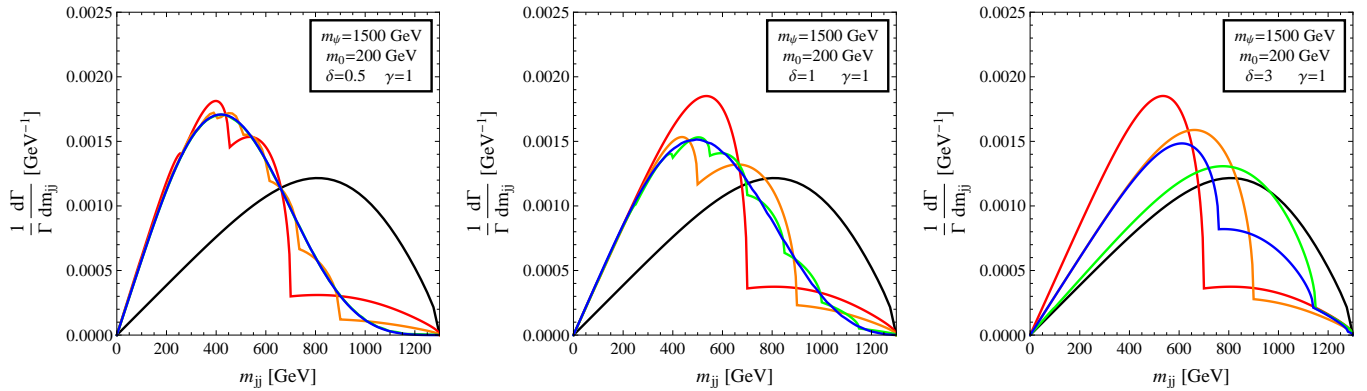


FIG. 4: DDM invariant-mass distributions, shown for increasing  $\delta$  with fixed  $m_\psi = 1500$  GeV,  $m_0 = 200$  GeV, and  $\gamma = 1$ . The results shown in the left, center, and right panels correspond to  $\delta = \{0.5, 1, 3\}$ , respectively. In each panel, the red, orange, green, and blue curves correspond to mass splittings  $\Delta m = \{600, 400, 150, 20\}$  GeV, respectively, while the black curve shows the result for a traditional dark-matter candidate with  $m_\chi = m_0$ .

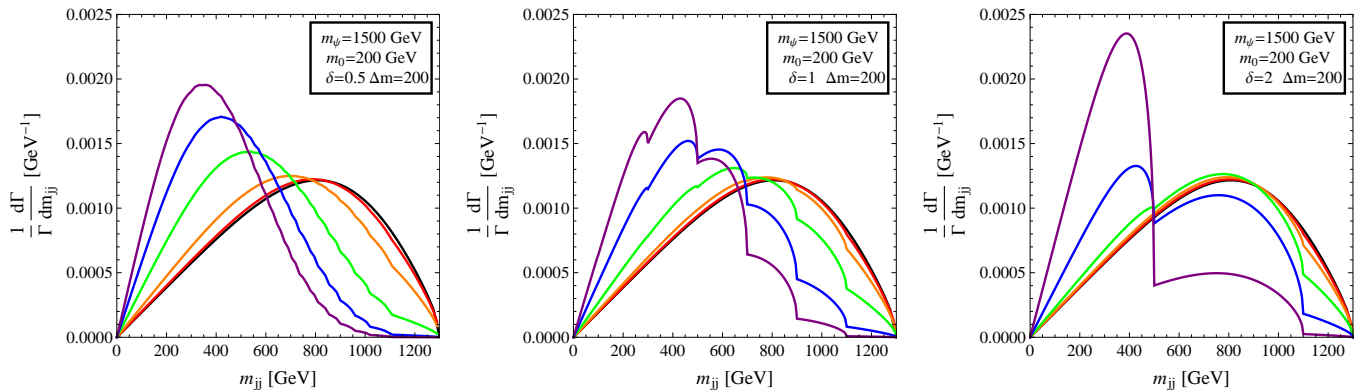


FIG. 5: DDM invariant-mass distributions, shown for increasing  $\delta$  with fixed  $m_\psi = 1500$  GeV,  $m_0 = 200$  GeV, and  $\Delta m = 200$  GeV. From top left to bottom right, the panels shown show results for  $\delta = \{0.5, 1, 2\}$ . In each panel, the red, orange, green, blue, and purple curves correspond to  $\gamma = \{-2, -1, 0, 1, 2\}$ , respectively, while the black curve shows the result for a traditional dark-matter candidate with  $m_\chi = m_0$ .

either  $\Delta m$  or  $\delta$  being sizeable. To some extent, this behavior is not unexpected, but the presence of such identifiable mass edges may ultimately provide one clear way of discerning a DDM ensemble experimentally. By contrast, in the opposite regime in which a large number of states contribute significantly to the decay width of the parent particle  $\psi$ , the  $m_{jj}$  distribution exhibits no identifiable edges, but instead assumes a unique shape which is markedly different from that observed in traditional dark-matter models. Such a shape emerges when mass splittings between the heavier states in the ensemble are small, and consequently a larger fraction of that ensemble (consisting primarily of the heavier  $\chi_n$ ) contributes non-trivially to the decay width of  $\psi$ .

#### IV. DISTINGUISHING DDM ENSEMBLES AT THE LHC

In the previous section, we examined a number of distinctive features which can emerge in the invariant-mass distributions associated with  $\psi \rightarrow jj\chi_n$  decays in DDM models. In this section, our primary aim is to assess the degree to which the characteristic  $m_{jj}$  distribution associated with a particular DDM model constitutes a distinctive signature of non-standard physics in the dark sector — *i.e.*, a signature that cannot be realized in any traditional dark-matter model, regardless of the mass  $m_\chi$  of the dark-matter candidate. Once again, for concreteness, we focus on the operator structure given in Eq. (3.6). In order to determine the statistical significance with which the  $m_{jj}$  distribution associated with any particular DDM model (*i.e.*, a particular set of values for the parameters  $m_\psi$ ,  $m_0$ ,  $\Delta m$ ,  $\gamma$ ,  $\delta$ ) is truly distinctive, we compare this distribution to the  $m_{jj}$  distributions associated with a variety of different traditional dark-matter models, each with a different value of  $m_\chi$ . In particular, we canvass the entire range  $0 < m_\chi < m_\psi - m_{jj}^{(\min)}$  with a finite step size. Note that we do *not* similarly scan over all possible spins combinations for  $\psi$  and  $\chi$ , or over coupling structures of these particles to SM quarks and gluons, but rather restrict our analysis to traditional dark-matter models in which the parent particle likewise decays via an operator of the form given in Eq. (3.4). This is justified because the shape of the  $m_{jj}$  distribution does not depend sensitively on the coupling structure, as we have demonstrated in Sect. III. We have nevertheless verified that our results do not differ significantly even if alternative coupling structures are incorporated into the analysis.

The procedure we adopt in comparing any two  $m_{jj}$  distributions is as follows. When  $m_{jj}$  is small, statistics are low and residual SM backgrounds are at their largest; we therefore begin by applying a minimum cut on  $m_{jj}$  of the form  $m_{jj} > m_{jj}^{(\min)}$ , where  $m_{jj}^{(\min)}$  is some particular invariant-mass threshold. We then partition the range of allowed dijet invariant masses  $m_{jj}^{(\min)} \leq m_{jj} \leq m_\psi - m_0$  into  $n_b$  bins whose widths vary with  $m_{jj}$ . Specifically, the width of each bin is taken to be equal to the dijet invariant-mass resolution  $\Delta m_{jj}$  at the minimum  $m_{jj}$  in the bin. We assume here that  $\Delta m_{jj}$  is limited predominately by the uncertainty  $\Delta E_j$  in the measurement of the energies  $E_j$  of the jets used in reconstructing  $m_{jj}$ , and hence we take  $(\Delta m_{jj})/m_{jj} \approx (\Delta E_j)/E_j$ . For the ATLAS detector, the jet-energy resolution has the rough scaling behavior [11]

$$\frac{\Delta E_j}{E_j} = 0.5 \left( \frac{E_j}{\text{GeV}} \right)^{-1/2} + 0.03, \quad (4.1)$$

and the jet-energy resolution at CMS is quite similar [12].

For each value of  $m_\chi$  in our survey, we assess the goodness of fit between the  $m_{jj}$  distributions associated with the specific DDM model under study and traditional dark-matter models by constructing the  $\chi^2$  statistic

$$\chi^2(m_\chi) = \sum_k \frac{[X_k - \mathcal{E}_k(m_\chi)]^2}{\sigma_k^2}, \quad (4.2)$$

where the index  $k$  labels the bin,  $X_k$  is the expected population of events in bin  $k$  in the DDM model,  $\mathcal{E}_k(m_\chi)$  is the expected population of events in bin  $k$  in a traditional dark-matter model in which the dark-matter particle has mass  $m_\chi$ , and  $\sigma_k^2$  is the variance in  $X_k$  due to statistical uncertainties. Since the  $X_k$  are distributed according to a multinomial distribution, it follows that  $\sigma_k^2 = X_k(1 - X_k/N_e)$ , where  $N_e$  denotes the total number of signal events in the sample. Note that the minimum from among these  $\chi^2(m_\chi)$  values embodies the degree of discrepancy between the  $m_{jj}$  distribution associated with the DDM model and that associated with the traditional dark-matter model which provides the best fit to that distribution. We therefore adopt

$$\chi_{\min}^2 \equiv \min_{m_\chi} \{ \chi^2(m_\chi) \} \quad (4.3)$$

as our final measure of the distinctiveness of the  $m_{jj}$  distribution associated with the DDM model. We further determine the statistical significance associated with a particular value of  $\chi_{\min}^2$  by first comparing this value to a  $\chi^2$

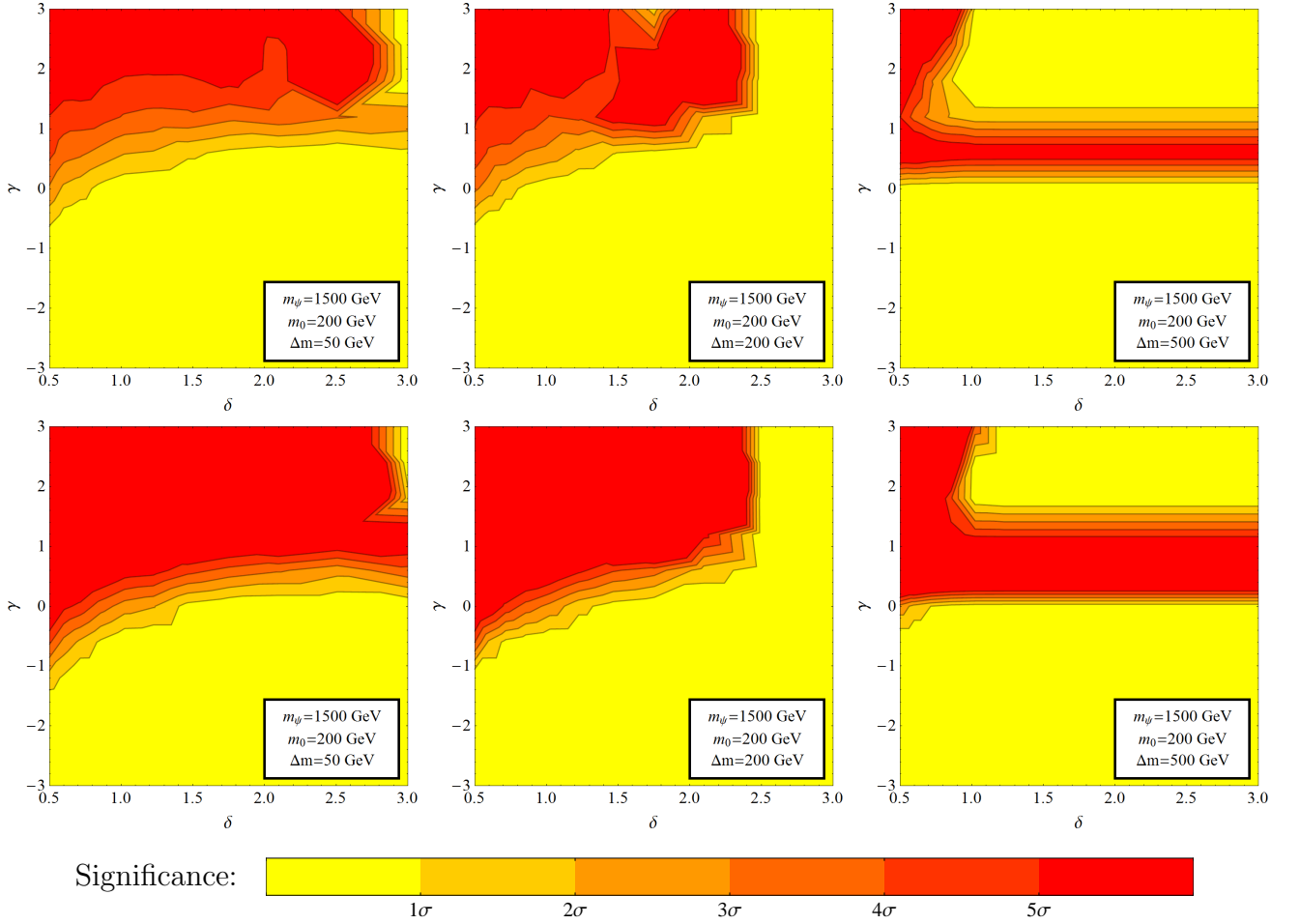


FIG. 6: Contour plots showing the minimum significance level at which the  $m_{jj}$  distribution predicted in the DDM model characterized by the parameters  $m_\psi$ ,  $m_0$ ,  $\Delta m$ ,  $\delta$ , and  $\gamma$  can be differentiated from the  $m_{jj}$  distribution predicted in any traditional dark-matter model. In the panels shown, we have fixed  $m_\psi = 1500$  GeV and  $m_0 = 200$  GeV, and taken  $m_{jj}^{(\min)} = 200$  GeV as our minimum  $m_{jj}$  threshold. The panels in the left column show results for  $\Delta m = 50$  GeV, the center column for  $\Delta m = 200$  GeV, and the right column for  $\Delta m = 500$  GeV. In each column, the top panel corresponds to  $N_e = 500$ , while the bottom panel corresponds to  $N_e = 1000$ .

distribution with  $n_b - 1$  degrees of freedom in order to obtain a  $p$ -value. We then take the significance level to be the number of standard deviations away from the mean to which the same  $p$ -value would correspond for a Gaussian distribution. Note that unlike in typical bump-hunting analyses, the  $p$ -value in this case is two-sided.

In Fig. 6, we show how the significance of differentiation varies as a function of  $\delta$  and  $\gamma$  with  $\Delta m$ ,  $m_0$ , and  $m_\psi$  held fixed. In all of the panels shown, we have set  $m_\psi = 1500$  GeV and  $m_0 = 200$  GeV, and we have taken  $m_{jj}^{(\min)} = 200$  GeV as our minimum  $m_{jj}$  threshold and a step size of 100 GeV in our scan over  $m_\chi$ . The panels in the left column show the results for  $\Delta m = 50$  GeV, the middle column for  $\Delta m = 200$  GeV, and the right column for  $\Delta m = 500$  GeV. In each column, the results shown in the top and bottom panels correspond to  $N_e = 500$  and  $N_e = 1000$ , respectively.

The results in the left column indicate that for relatively small  $\Delta m$ , our DDM model can be distinguished from traditional dark-matter scenarios at a significance level of  $5\sigma$  or higher for  $\gamma \gtrsim 0.5$  and  $\delta \lesssim 3$  with  $N_e \gtrsim 1000$ . This is due to the fact that the coupling to the heavier  $\chi_n$  are proportionally larger for  $\gamma > 0$ , and these states increasingly dominate the width of  $\psi$  as  $\gamma$  increases. As a result, the peak of the  $m_{jj}$  distribution shifts to smaller values of  $m_{jj}$ , and is therefore more readily distinguished from the distribution obtained in traditional dark-matter models. By contrast, for  $\gamma < 0$ , the width of  $\psi$  is dominated by decays to the lighter  $\chi_n$ , and the  $m_{jj}$  distributions obtained in this regime resemble much more closely those associated with traditional dark-matter models. This behavior is evident in the center and right panels as well.

We also see from the panels of Fig. 6 that the significance for differentiation depends non-trivially on  $\delta$  and  $\Delta m$  as well. For example, an increase in significance within the  $\gamma < 0$  region is obtained for small  $\delta$  — an increase which is particularly pronounced for small  $\Delta m$ . This effect is a consequence of the sheer multiplicity of heavy  $\chi_n$  overwhelming the effect of the coupling suppression of  $\psi$  to these states (which occurs for  $\gamma < 0$ ) and resulting in a  $m_{jj}$  distribution which peaks at far smaller values of  $m_{jj}$  than in traditional dark-matter models. Conversely, in the opposite regime in which  $\gamma > 0$  and  $\delta$  is large, a precipitous drop in the significance occurs for  $\delta \gtrsim 3$  in the  $\gamma \gtrsim 0.5$  region for  $\Delta m = 50$  GeV, and at even smaller values of  $\delta$  for larger  $\Delta m$ . This behavior reflects the fact that as  $\Delta m$  and  $\delta$  increase, the mass splittings between the  $\chi_n$  eventually become larger, and consequently fewer and fewer  $\chi_n$  remain kinematically accessible in  $\psi$  decays. In such cases, the contribution from either of these states can mimic the  $m_{jj}$  distribution obtained for a single dark-matter particle, depending on the branching fractions  $\text{BR}_{\psi 0}$  and  $\text{BR}_{\psi 1}$ . Whenever  $\text{BR}_{\psi 0} \gg \text{BR}_{\psi 1}$  or  $\text{BR}_{\psi 0} \ll \text{BR}_{\psi 1}$ , only one of these two particles dominates the width of  $\psi$ , and the resulting  $m_{jj}$  distribution resembles that obtained for a traditional dark-matter candidate with  $m_\chi = m_0$  or  $m_\chi = m_1$ , respectively. However, in situations in which  $\text{BR}_{\psi 0} \sim \text{BR}_{\psi 1}$  and both particles have a salient effect on the  $m_{jj}$  distribution, it takes a shape which no single-particle dark-matter candidate can replicate. Since the relationship between these branching fractions is primarily governed by  $\gamma$ , there exists a narrow range  $0 \lesssim \gamma \lesssim 1$  within which the significance for differentiation is substantial for large  $\delta$  and  $\Delta m$ . By contrast, outside of this region, either  $\chi_0$  or  $\chi_1$  overwhelmingly dominates the width of  $\psi$ , and the significance drops dramatically. Indeed, this behavior is evident in the right panels of Fig. 6.

The plots in each column of Fig. 6 illustrate the effect of  $N_e$  on the significance of differentiation, and in particular on the sensitivity of our results to the total event count. Indeed, we observe that a  $5\sigma$  significance of differentiation is achieved over a substantially larger region of parameter space for  $N_e = 1000$  than for  $N_e = 500$ . Moreover, it turns out that the region of parameter space in which such a significance is obtained diminishes rapidly with decreasing  $N_e$  for  $N_e \lesssim 500$ . Thus, we conclude that  $N_e \sim \mathcal{O}(500 - 1000)$  is roughly the size of the data sample for which  $m_{jj}$  distributions begin to provide significant resolving power between DDM scenarios and traditional dark-matter models. In Sect. V, we shall provide an example of a production mechanism which naturally yields such  $N_e$  values for  $\mathcal{L}_{\text{int}} = 30 \text{ fb}^{-1}$  at the  $\sqrt{s} = 14$  TeV LHC.

In Fig. 7, we show how the significance of differentiation varies as a function of  $\Delta m$  and  $\delta$  with  $\gamma$ ,  $m_0$ , and  $m_\psi$  held fixed. The results shown correspond to the same choices of  $m_\psi$ ,  $m_0$ ,  $m_{jj}^{(\text{min})}$ , and step size for  $m_\chi$  as in Fig. 6. The left, center, and right panels show the results for  $\gamma = \{-1, 0, 1\}$ , respectively. Once again, we see from the left panel that for  $\gamma < 0$ , the density of states as a function of mass within the DDM ensemble must increase quite rapidly with  $n$  to overcome the corresponding coupling suppression. Both  $\Delta m$  and  $\delta$  must be extremely small for this to occur. As  $\gamma$  increases, less extreme values for these parameters are required to overcome the coupling suppression, as the results shown in the center panel of the figure attest. A horizontal band of slightly increased significance for  $300 \text{ GeV} \lesssim \Delta m \lesssim 450 \text{ GeV}$  is also evident for  $\delta \gtrsim 1.5$ . This once again corresponds to the region of parameter space discussed above, within which  $\chi_0$  and  $\chi_1$  are the only states in the ensemble kinematically accessible in  $\psi$  decays, but within which the  $m_{jj}$  distribution nevertheless differs significantly from those associated with traditional dark-matter candidates because  $\text{BR}_{\psi 0} \sim \text{BR}_{\psi 1}$ . In the right panel, the couplings of the heavier  $\chi_n$  are enhanced relative to those of their lighter counterparts, and as a result, the only regions of parameter space shown in which a  $5\sigma$  significance is not obtained are those which correspond to the upper right portions of the  $\Delta m = 50$  GeV and  $\Delta m = 200$  GeV panels in Fig. 6, within which only two of the  $\chi_n$  are kinematically accessible in  $\psi$  decays, and one of these two particles overwhelmingly dominates the width of  $\psi$ .

Finally, in Fig. 8, we show how the significance of differentiation varies as a function of  $\Delta m$  and  $\gamma$  with  $\delta$ ,  $m_0$ , and  $m_\psi$  held fixed. Once again, the results shown correspond to the same choices of  $m_\psi$ ,  $m_0$ ,  $m_{jj}^{(\text{min})}$ , and step size for  $m_\chi$  as in Fig. 6. The left, center, and right panels show the results for  $\delta = \{0.5, 1, 2\}$ , respectively. The results in these panels illustrate once again that large  $\gamma$  generally yields a large significance for differentiation — except in situations in which  $\chi_0$  and  $\chi_1$  are the only  $\chi_n$  sufficiently light to be produced by  $\psi$  decays, and the condition  $\text{BR}_{\psi 0} \sim \text{BR}_{\psi 1}$  must be satisfied in order for the  $m_{jj}$  distribution to differ significantly from that of a traditional dark-matter model with either  $m_\chi = m_0$  or  $m_\chi = m_1$ .

Taken together, the results displayed in Figs. 6 through 8 indicate that it is possible to discriminate between a wide range of DDM ensembles and more traditional dark-matter candidate on the basis of dijet invariant-mass distributions at the LHC. Indeed, we have shown that a statistical significance for discrimination in excess of  $5\sigma$  is obtained for  $N_e = 1000$  over a broad region of the DDM model parameter space, and regions of parameter space within which  $\gamma$  is large or within which  $\Delta m$  is small and  $\delta < 1$  are particularly auspicious.

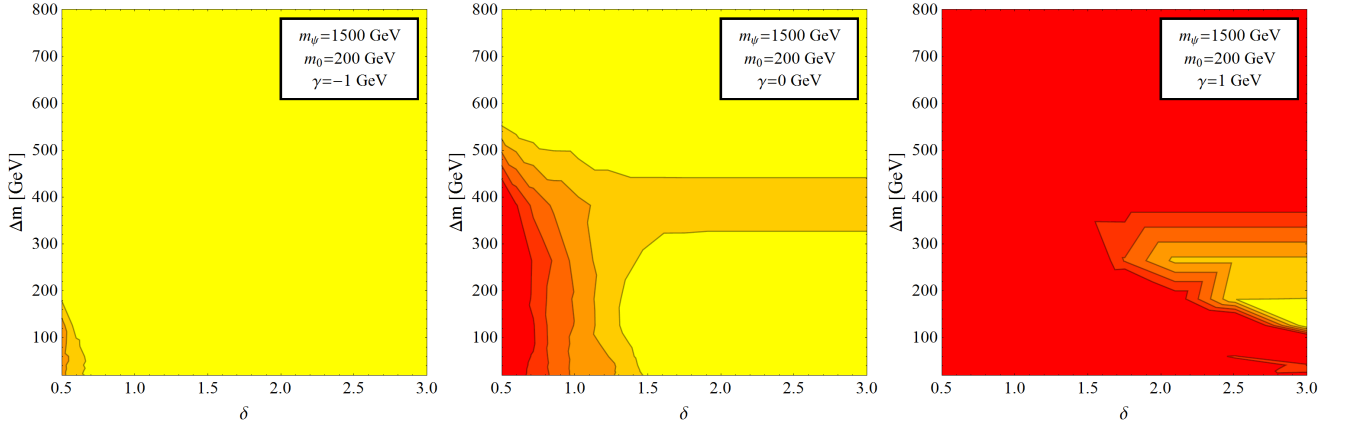


FIG. 7: Contour plots showing the minimum significance level at which the  $m_{jj}$  distribution predicted in the DDM model characterized by the parameters  $m_\psi$ ,  $m_0$ ,  $\Delta m$ ,  $\delta$ , and  $\gamma$  can be differentiated from the  $m_{jj}$  distribution predicted in any traditional dark-matter model for  $N_e = 1000$ . The colored regions shown correspond to the same significance intervals as in Fig. 6, and the results shown correspond to the same values of  $m_\psi$ ,  $m_0$ , and  $m_{jj}^{(\min)}$ . The left panel shows results for  $\gamma = -1$ , the center panel for  $\gamma = 0$ , and the right panel for  $\gamma = 1$ .

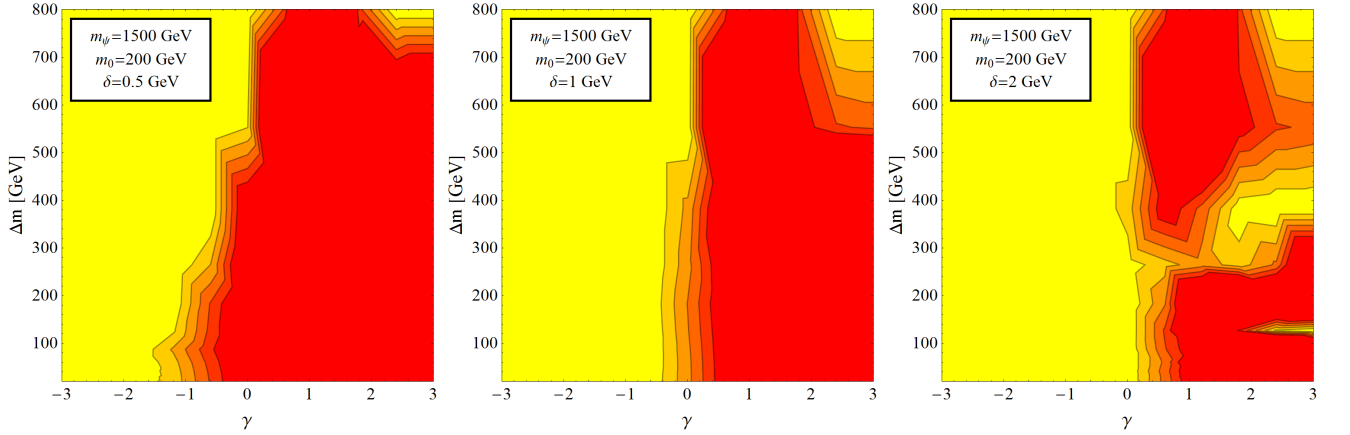


FIG. 8: Contour plots showing the minimum significance level at which the  $m_{jj}$  distribution predicted in the DDM model characterized by the parameters  $m_\psi$ ,  $m_0$ ,  $\Delta m$ ,  $\delta$ , and  $\gamma$  can be differentiated from the  $m_{jj}$  distribution predicted in any traditional dark-matter model for  $N_e = 1000$ . The colored regions shown correspond to the same significance intervals as in Fig. 6, and the results shown correspond to the same values of  $m_\psi$ ,  $m_0$ , and  $m_{jj}^{(\min)}$ . The left panel shows results for  $\delta = 0.5$ , the center panel for  $\delta = 1$ , and the right panel for  $\delta = 2$ .

## V. DDM PRODUCTION CHANNELS AND EVENT RATES

Thus far, we have not specified any particular production mechanism for the parent particle  $\psi$  whose decays give rise to the constituent fields of the DDM ensemble. Indeed, all of our results up to this point have been essentially independent of the details of the mechanism by which the  $\psi$  are produced, provided that the SM background can be reduced to a negligible level by cuts imposed on the data and that jets associated with the decay of each parent particle can be correctly identified. Indeed, they depend only on the total event count  $N_e$ . This gives our analysis a broad range of applicability. We have demonstrated that in a wide variety of situations,  $N_e \sim \mathcal{O}(500 - 1000)$  is sufficient to distinguish a DDM ensemble from a traditional dark-matter candidate at the  $5\sigma$  significance level. It is therefore natural to wonder whether such values of  $N_e$  might reasonably be expected within the next few years of operation at the LHC, and what sorts of parent-particle production processes are capable of yielding such event counts.

In this section, we provide an example of a production process which generically yields event counts of this order

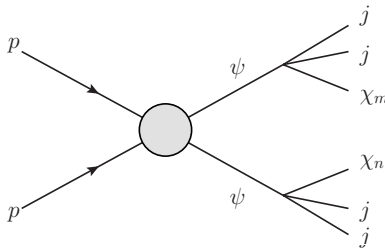


FIG. 9: One possible DDM production channel: the pair production of heavy states which decay into four jets and a pair of DDM-ensemble constituents.

for any strongly-interacting parent particle with a TeV-scale mass: the pair-production of  $\psi$ , as indicated in Fig. 9. Indeed, any strongly-interacting exotic can be produced in this manner, via its interactions with the gluon field. While the precise value of  $N_e$  in any particular case depends on the chosen Lorentz and  $SU(3)_c$  representations of  $\psi$ , on the value of  $m_\psi$ , and on the event-selection criteria imposed, we shall now demonstrate that event counts of the order assumed in Sect. IV can easily be obtained with an integrated luminosity of roughly  $\mathcal{L}_{\text{int}} \sim 30 \text{ fb}^{-1}$  at the  $\sqrt{s} = 14 \text{ TeV}$  LHC.

For any process via which  $\psi$  is produced at colliders, the expected number of signal events  $N_e$  surviving all cuts imposed on the data is given by

$$N_e = N_\psi \sigma_\psi \mathcal{L}_{\text{int}} A \epsilon_{\text{sig}} \sum_n \text{BR}(\psi \rightarrow jj\chi_n), \quad (5.1)$$

where  $\mathcal{L}_{\text{int}}$  is the integrated luminosity,  $A$  is the detector acceptance,  $\epsilon_{\text{sig}}$  is the signal-event-selection efficiency,  $\sigma_\psi$  is the cross-section for the production process in question, and  $N_\psi$  is the multiplicity of  $\psi$  particles produced in each event. For pair production, of course,  $N_\psi = 2$ . Note that in assessing  $\epsilon_{\text{sig}}$  for any particular production mechanism, we stipulate that the corresponding event-selection efficiency for the SM background is such that this background is negligible. Moreover, in what follows, we shall assume for simplicity that the total branching fraction of  $\psi$  to final states consisting of a pair of jets and one of the  $\chi_n$  is effectively unity. With these assumptions, the contribution to  $N_e$  from pair production depends simply on the total pair-production cross-section  $\sigma_{pp \rightarrow \psi\psi}$  for  $\psi$ , on the cuts imposed on the data (through  $\epsilon_{\text{sig}}$ ), and on the inherent properties of the detector (through  $A$ ).

We begin by evaluating  $\sigma_{pp \rightarrow \psi\psi}$ . The parton-level pair-production cross-sections  $\sigma_{\bar{q}q \rightarrow \psi\psi}$  and  $\sigma_{gg \rightarrow \psi\psi}$  for an exotic scalar or fermion which transforms in an arbitrary representation of  $SU(3)_c$  were calculated to leading order (LO) in Ref. [13]. Convolving these expressions with the appropriate parton-distribution functions (PDFs) in each case yields the LO hadronic cross-section  $\sigma_{pp \rightarrow \psi\psi}$ . In this analysis, we use the CTEQ6L1 [14] PDF set, and impose a pseudorapidity cutoff  $|\eta| \leq 3$  in computing the hadronic cross-sections in order to account for the finite pseudorapidity coverage of the LHC detectors. The LO hadronic cross-sections corresponding to several combinations of  $SU(3)_c$  and Lorentz representations for  $\psi$  for which decays of the form  $\psi \rightarrow jj\chi_n$  can have sizeable branching fractions are shown in the left panel of Fig. 10 as a function of  $m_\psi$ . We see from this figure that in the case in which  $\psi$  is a Majorana fermion transforming in the **8** representation of  $SU(3)_c$  or a Dirac fermion transforming in the **15** representation, a cross section in the range  $\sigma_{pp \rightarrow \psi\psi} \gtrsim 100 \text{ fb}$  is attained for all values of  $m_\psi \lesssim \{1100, 1500\} \text{ GeV}$  at the  $\sqrt{s} = 14 \text{ TeV}$  LHC. While the cross-sections are smaller for the cases in which  $\psi$  is a scalar field transforming in the **3** or **6** representation of  $SU(3)_c$ , they are still be reasonably large for  $m_\psi \lesssim 1000 \text{ GeV}$ .

We now turn to address the values of  $A$  and  $\epsilon_{\text{sig}}$  associated with the pair-production of a strongly-interacting parent particle. Since  $\epsilon_{\text{sig}}$  depends sensitively on the details of the scenario in question and on the particular set of event-selection criteria which provides an optimal discriminant between signal and background in that scenario, we focus on one representative example case: that in which  $\psi$  is a color-octet Majorana fermion. For this case, representative values for the product  $A\epsilon_{\text{sig}}$  may be taken from results of searches for pair-produced gluinos by the ATLAS collaboration [15, 16] in the jets +  $\cancel{E}_T$  channel in the regime in which all squarks are taken to be heavy. Specifically, we adopt the efficiencies obtained for a number  $N_j \geq 3$  of high- $p_T$  jets and  $m_{\text{eff}} > 500 \text{ GeV}$ , where  $m_{\text{eff}}$  is the scalar sum of  $\cancel{E}_T$  and the magnitudes  $p_{T_j}$  of the transverse momenta of the three leading jets in the event, ranked by  $p_T$ . In either case,  $A\epsilon_{\text{sig}}$  lies within the range  $0.3 - 0.6$  for  $m_\psi \gtrsim 500 \text{ GeV}$ . In addition, an estimate of the effects of next-to-leading-order (NLO) corrections to  $\sigma_{pp \rightarrow \psi\psi}$  in this case can be obtained using the  $K$ -factor formalism, in which the LO cross-section is scaled by an overall multiplier. The NLO  $K$ -factors for  $\psi$  pair production used in this analysis were obtained using the Prospino package [17], and vary from  $K \approx 1.7 - 4.4$  for  $300 \lesssim m_\psi \lesssim 2500 \text{ GeV}$  at  $\sqrt{s} = 8 \text{ TeV}$  and from  $K \approx 1.5 - 2.1$  at  $\sqrt{s} = 14 \text{ TeV}$  for the same mass range.

In the right panel of Fig. 10, we show the expected number  $N_e$  of events at the ATLAS detector for the case in

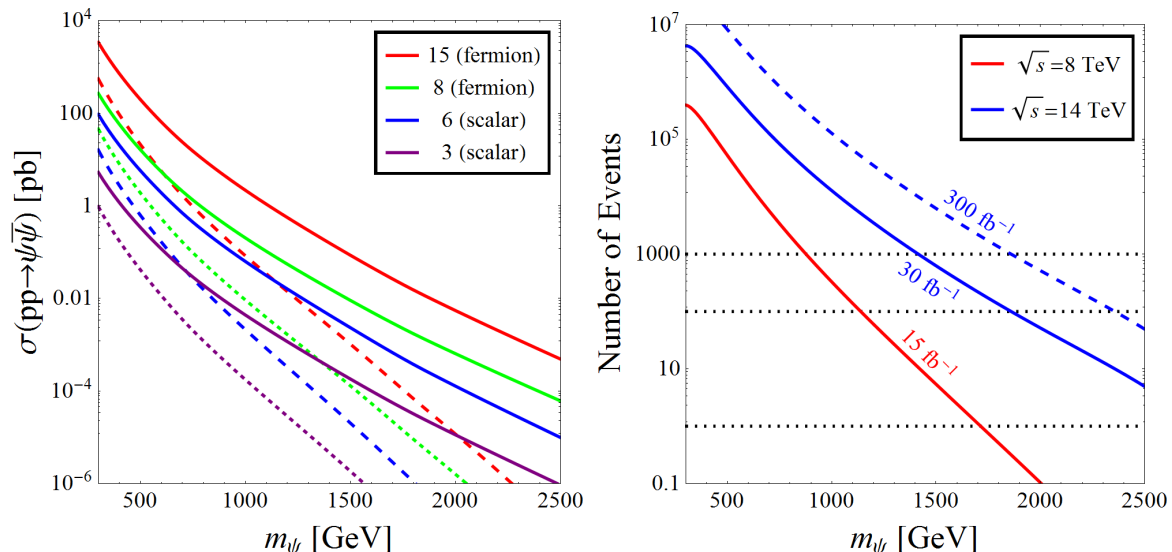


FIG. 10: *Left panel:* The pair-production cross-sections  $\sigma_{pp \rightarrow \psi\bar{\psi}}$  obtained for a variety of relevant combinations of  $SU(3)_c$  and Lorentz representations for a strongly-interacting parent particle  $\psi$ . The labels shown in the legend indicate the dimension of the  $SU(3)_c$  representation for  $\psi$  in each case, as well as whether  $\psi$  is a scalar (as in the **3** and **6** cases shown), a Majorana fermion (as in the **8** case), or a Dirac fermion (as in the **15** case). The dashed curves indicate the results for  $\sqrt{s} = 8$  TeV, while the solid curves indicate the results for  $\sqrt{s} = 14$  TeV. *Right panel:* the expected number of pair-production events  $N_e$  (taking into account detector acceptance and signal efficiency) for a color-octet Majorana fermion  $\psi$ , plotted as a function of its mass  $m_\psi$  for a variety of different integrated luminosities at the LHC. The red curve corresponds to  $\mathcal{L}_{\text{int}} = 15 \text{ fb}^{-1}$  at  $\sqrt{s} = 8$  TeV. The two blue curves correspond to  $\mathcal{L}_{\text{int}} = 30 \text{ fb}^{-1}$  (solid curve) and  $\mathcal{L}_{\text{int}} = 300 \text{ fb}^{-1}$  (dashed curve) at  $\sqrt{s} = 14$  TeV. Dotted horizontal lines indicating  $N_e = \{1, 100, 1000\}$  have also been included for convenience. We thus see that significant values of  $N_e$  can easily be achieved at the LHC through this production mechanism.

which  $\psi$  is a color-octet Majorana fermion, plotted as a function of  $m_\psi$  with  $\mathcal{L}_{\text{int}} = 15 \text{ fb}^{-1}$  for the current LHC run at  $\sqrt{s} = 8$  TeV (red), and with  $\mathcal{L}_{\text{int}} = \{30, 300\} \text{ fb}^{-1}$  for the projected upcoming run at  $\sqrt{s} = 14$  TeV (blue). These results incorporate the effects of detector acceptance and signal efficiency, as discussed above, and include the relevant NLO  $K$ -factors. Dotted lines corresponding to  $N_e = \{1, 100, 1000\}$  have also been included for reference. Note that for this choice of representations,  $m_\psi$  is constrained by ATLAS gluino searches [18] in the jets +  $\cancel{E}_T$  channel in the context of supersymmetric models with heavy, decoupled squarks. Such searches likewise place a constraint  $m_\psi \gtrsim 700$  GeV on the mass of any color-octet Majorana fermion which decays to a pair of jets and an invisible particle with a branching fraction near unity.

The results displayed in the right panel of Fig. 10 demonstrate that the pair-production of strongly-interacting parent particles with TeV-scale masses is certainly capable of yielding  $N_e \sim \mathcal{O}(500 - 1000)$  within the first  $30 \text{ fb}^{-1}$  of integrated luminosity at the  $\sqrt{s} = 14$  TeV LHC — an event count which was shown in Sect. IV to be sufficient for conclusively distinguishing DDM scenarios from more traditional dark-matter models on the basis of  $m_{jj}$  distributions. Indeed, we see that  $N_e \sim 1000$  can be expected for a color-octet fermion parent particle with  $m_\psi \lesssim 1500$  GeV at such an integrated luminosity during the planned run at  $\sqrt{s} = 14$  TeV. Furthermore, even with the integrated luminosity  $\mathcal{L}_{\text{int}} \approx 15 \text{ fb}^{-1}$  anticipated by the conclusion of the current run at  $\sqrt{s} = 8$  TeV, an event count of roughly  $N_e \sim 1000$  is obtained for  $m_\psi \lesssim 800$  GeV. While acceptance and signal-efficiency factors will differ somewhat for parent particles with different spins and  $SU(3)_c$  representations, the results shown in the left panel of Fig. 10 indicate that event counts of this order can likewise be expected in a variety of other cases as well. It should be noted, however, that combinatorial ambiguities associated with the pairing of final-state jets frequently necessitate the imposition of additional cuts, and this can lead to a reduction in signal efficiency. In Sect. VI, we shall discuss various methods through which such combinatorial ambiguities can be addressed.

## VI. DISCUSSION AND CONCLUSIONS

In this paper, we have examined the prospects for observing evidence of dynamical dark matter at colliders, and for distinguishing between DDM scenarios and more traditional dark-matter scenarios on the basis of collider data.



We have focused primarily on one promising technique: the identification of distinctive features imprinted on the kinematic distributions of SM fields produced along with the constituent fields of the DDM ensemble via the decays of other, heavier fields which happen to be present in a given DDM model. We have shown that the distributions which arise in DDM models can differ substantially from the characteristic distributions which arise in traditional dark-matter models in which a single stable, neutral beyond-the-SM particle is responsible for essentially the entirety of  $\Omega_{\text{CDM}}$ . To illustrate the efficacy of our approach, we have examined the prospects for observing a statistically significant deviation in the shape of the dijet invariant-mass distributions obtained for a particular representative DDM scenario relative to those obtained in traditional dark-matter models. We have demonstrated that throughout a substantial region of the parameter space of our scenario, a deviation at the  $5\sigma$  level is obtained within the first  $30 \text{ fb}^{-1}$  of integrated luminosity at the  $\sqrt{s} = 14 \text{ TeV}$  LHC. In particular, we have shown that regions of the parameter space of this scenario in which  $\gamma > 0$  or in which  $\Delta m$  is small and  $\delta < 1$  are particularly auspicious for differentiation. These findings confirm that the LHC is capable of providing compelling evidence for dynamical dark matter within the next few years.

We emphasize that the quantitative results we have obtained depend primarily on the total production rate for the parent particle and not on the particular manner in which this parent particle is produced. Indeed, these results apply directly to any situation in which the jets produced by the decay of each parent particle  $\psi$  in the event can be unambiguously identified with that particular  $\psi$ . In certain cases, such identification is indeed trivial. For example,  $\psi$  may be produced singly or have competing decays. Moreover, even in situations in which  $\psi$  decays predominately via parton-level processes of the form  $\psi \rightarrow \bar{q}q\chi_n$ , heavy-flavor tagging could assist in the identification of the correct pairings in events in which one parent particle decays to a final state involving light quarks and the other to a final state involving heavy quarks, *e.g.*,  $\bar{b}b$ . In many situations, however, it is not possible to identify the correct pairing of final-state jets based on the properties of the jets alone, and incorrect jet pairings give rise to a substantial combinatorial background. Nevertheless, a number of techniques exist for eliminating this combinatorial background. These include the hemisphere method [19, 20], the use of additional kinematic variables such as  $m_{T_2}$  [21], and background-subtraction strategies [22]. Indeed, it would be interesting to assess the relative efficacy of these techniques in helping to discriminate between DDM models and more traditional dark-matter scenarios in the presence of combinatorial ambiguities [23].

We note that we have chosen to focus on the case in which the SM particles produced alongside the  $\chi_n$  by  $\psi$  decays are quarks or gluons solely because large event rates can generically be expected for strongly-interacting  $\psi$ . However, the techniques that we have developed here can also be applied to situations in which  $\psi$  decays to final states involving different combinations of SM particles as well. For example, the prospects for differentiating between DDM scenarios and traditional dark-matter models obtained for decay topologies such as  $\psi \rightarrow \ell^+\ell^-\chi_n$ , where  $\ell^\pm$  denotes a charged lepton, will be identical to those obtained for  $\psi \rightarrow jj\chi_n$ , given the same total number of events  $N_e$ .

We also note that the techniques outlined here for differentiating between DDM ensembles and more traditional dark-matter candidates also have a range of applicability that extends beyond the DDM framework. Indeed, not every particle which manifests itself as  $\cancel{E}_T$  at colliders necessarily contributes significantly (or at all) to  $\Omega_{\text{CDM}}$ , and  $\cancel{E}_T$  signatures of this sort can arise in a number of theories involving multiple neutral particles which are stable on collider time scales but not necessarily stable on time scales approaching the age of the universe. As discussed in Sect. II, examples of such theories can be found among supersymmetric models with highly compressed spectra [25], scenarios involving universal extra dimensions [8–10], and a wide variety of additional extensions of the SM.

Finally, we note that in this paper we have focused on the case in which  $\psi$  decays to a final state consisting of SM states and one or more of the  $\chi_n$  directly, via an effective multi-body interaction vertex. Alternatively, one could also consider the situation in which  $\psi$  decays to such a final state primarily via decay chains involving on-shell intermediate states. Indeed, the kinematic distributions associated with the final-state SM fields in this latter case differ significantly from those obtained in the former. For example, in traditional dark-matter models, the  $m_{jj}$  distributions associated with  $\psi \rightarrow jj\chi$  processes which proceed via cascade decays involving an on-shell intermediary take a characteristic triangular shape. It would be interesting to examine the corresponding  $m_{jj}$  distributions which arise for DDM ensembles, and whether such dark-matter candidates can likewise conclusively be distinguished from traditional dark-matter candidates on the basis of these distributions [24].

### Acknowledgments

We would like to thank Z. Chacko, J. Rutherford, S. Vahsen, and E. Varnes for discussions. KRD and SS are supported in part by the U.S. Department of Energy under Grant DE-FG02-04ER-41298, and KRD is additionally supported in part by the National Science Foundation through its employee IR/D program. BT is supported in part by DOE grant DE-FG02-04ER-41291. The opinions and conclusions expressed here are those of the authors, and do not represent either the Department of Energy or the National Science Foundation.



- 
- [1] K. R. Dienes and B. Thomas, “Dynamical Dark Matter: I. Theoretical Overview,” arXiv:1106.4546 [hep-ph], to appear in Phys. Rev. D.
- [2] K. R. Dienes and B. Thomas, “Dynamical Dark Matter: II. An Explicit Model,” arXiv:1107.0721 [hep-ph], to appear in Phys. Rev. D.
- [3] K. R. Dienes and B. Thomas, “Phenomenological Constraints on Axion Models of Dynamical Dark Matter,” arXiv:1203.1923 [hep-ph].
- [4] For recent reviews, see, *e.g.*,  
 G. Jungman, M. Kamionkowski and K. Griest, Phys. Rept. **267**, 195 (1996) [arXiv:hep-ph/9506380];  
 K. A. Olive, arXiv:astro-ph/0301505;  
 D. Hooper, arXiv:0901.4090 [hep-ph];  
 N. Weiner, “Dark Matter Theory,” video lectures given at TASI 2009,  
[http://physicslearning2.colorado.edu/tasi/tasi\\_2009/tasi\\_2009.htm](http://physicslearning2.colorado.edu/tasi/tasi_2009/tasi_2009.htm);  
 J. L. Feng, Ann. Rev. Astron. Astrophys. **48**, 495 (2010) [arXiv:1003.0904 [astro-ph.CO]].
- [5] K. Agashe, D. Kim, M. Toharia and D. G. E. Walker, Phys. Rev. D **82**, 015007 (2010) [arXiv:1003.0899 [hep-ph]].
- [6] K. Agashe, D. Kim, D. G. E. Walker and L. Zhu, Phys. Rev. D **84**, 055020 (2011) [arXiv:1012.4460 [hep-ph]].
- [7] G. Servant and T. M. P. Tait, Nucl. Phys. B **650**, 391 (2003) [arXiv:hep-ph/0206071];  
 H. C. Cheng, J. L. Feng and K. T. Matchev, Phys. Rev. Lett. **89**, 211301 (2002) [arXiv:hep-ph/0207125].
- [8] I. Antoniadis, Phys. Lett. B **246**, 377 (1990);  
 I. Antoniadis, K. Benakli and M. Quiros, Phys. Lett. B **331**, 313 (1994) [arXiv:hep-ph/9403290].
- [9] K. R. Dienes, E. Dudas and T. Gherghetta, Phys. Lett. B **436**, 55 (1998) [arXiv:hep-ph/9803466]; Nucl. Phys. B **537**, 47 (1999) [arXiv:hep-ph/9806292]; arXiv:hep-ph/9807522.
- [10] T. Appelquist, H. C. Cheng and B. A. Dobrescu, Phys. Rev. D **64**, 035002 (2001) [arXiv:hep-ph/0012100].
- [11] “ATLAS: Detector and physics performance technical design report. Volume 1,” CERN-LHCC-99-14.
- [12] V. Khachatryan *et al.* [CMS Collaboration], Phys. Rev. Lett. **105**, 211801 (2010) [arXiv:1010.0203 [hep-ex]];  
 S. Chatrchyan *et al.* [CMS Collaboration], Phys. Lett. B **700**, 187 (2011) [arXiv:1104.1693 [hep-ex]].
- [13] J. Kumar, A. Rajaraman and B. Thomas, Phys. Rev. D **84**, 115005 (2011) [arXiv:1108.3333 [hep-ph]].
- [14] J. Pumplin, D. R. Stump, J. Huston, H. L. Lai, P. M. Nadolsky and W. K. Tung, JHEP **0207**, 012 (2002) [arXiv:hep-ph/0201195].
- [15] G. Aad *et al.* [Atlas Collaboration], Phys. Lett. B **701**, 186 (2011) [arXiv:1102.5290 [hep-ex]].
- [16] See <http://hepdata.cedar.ac.uk/resource/atlas/>.
- [17] W. Beenakker, R. Hopker, M. Spira and P. M. Zerwas, Nucl. Phys. B **492**, 51 (1997) [arXiv:hep-ph/9610490];  
 W. Beenakker, M. Kramer, T. Plehn, M. Spira and P. M. Zerwas, Nucl. Phys. B **515**, 3 (1998) [arXiv:hep-ph/9710451].
- [18] G. Aad *et al.* [ATLAS Collaboration], arXiv:1109.6572 [hep-ex].
- [19] W. S. Cho, K. Choi, Y. G. Kim and C. B. Park, JHEP **0802**, 035 (2008) [arXiv:0711.4526 [hep-ph]];  
 M. M. Nojiri, Y. Shimizu, S. Okada and K. Kawagoe, JHEP **0806**, 035 (2008) [arXiv:0802.2412 [hep-ph]];  
 M. M. Nojiri, K. Sakurai, Y. Shimizu and M. Takeuchi, JHEP **0810**, 100 (2008) [arXiv:0808.1094 [hep-ph]];  
 S. -G. Kim, N. Maekawa, K. I. Nagao, M. M. Nojiri and K. Sakurai, JHEP **0910**, 005 (2009) [arXiv:0907.4234 [hep-ph]].
- [20] A. Rajaraman and F. Yu, Phys. Lett. B **700**, 126 (2011) [arXiv:1009.2751 [hep-ph]].
- [21] C. G. Lester and D. J. Summers, Phys. Lett. B **463**, 99 (1999) [arXiv:hep-ph/9906349];  
 A. Barr, C. Lester and P. Stephens, J. Phys. G **29**, 2343 (2003) [arXiv:hep-ph/0304226].
- [22] B. Dutta, T. Kamon, N. Kolev and A. Krislock, Phys. Lett. B **703**, 475 (2011) [arXiv:1104.2508 [hep-ph]].
- [23] K. R. Dienes, J. Rutherford, S. Su and B. Thomas, in preparation.
- [24] K. R. Dienes, S. Su and B. Thomas, in preparation.
- [25] S. P. Martin, Phys. Rev. D **75**, 115005 (2007) [arXiv:hep-ph/0703097].